Strojnícky časopis – *Journal of* MECHANICAL ENGINEERING,
VOL 75 (2025), NO 3, 53 - 62

# FEM ANALYZES AND EXPERIMENTAL VERIFICATION OF THE LOAD CAPACITY OF PRESTRESSED BOLTED JOINTS OF PHOTOVOLTAIC PANELS DYNAMICALLY LOADED BY WIND

**MUÑIZ-CALVENTE Miguel[1], DÍAZ-SALAMANCA Diego[1], KANAVAL Antonín[2], KANAVAL Jan[2*]**

[1]*University of Oviedo, Department of Construction and Manufacturing Engineering, Gijón 33203, Spain*
[2]*Faculty of Mechanical Engineering, Czech Technical University in Prague, Dept. of Designing and Mechanical Components, Technická 4 ,166 07 Prague 6, Czech Republic, e – mail: jan.kanaval@fs.cvut.cz*

**Abstract:** Nowadays, the use of hot-dip galvanized prestressed bolted joints has greatly increased in many industrial applications, especially in the solar generation industry The expansion of the use of these joints has occurred due to their excellent resistance to atmospheric corrosion and also because of their easy assembly and maintenance at relatively low costs. However, the fatigue behavior of these joints is still not sufficiently experimentally verified and defined in design standards, which makes their correct dimensioning difficult.

**KEYWORDS:** Hot-dip Galvanized Prestressed Bolted Joint; Fatigue Behavior; Solar Generation Industry; Wind Loading of Photovoltaic Panels

## 1 Introduction

This work mainly deals with the analysis of hot-dip prestressed bolted joints used for fastening photovoltaic panels loaded by wind in terms of the fasteners used and the suitability of the proposed design solution. Furthermore, this work marginally describes the performed FEM analyses and experiments that evaluate different geometric configurations of the connection, such as slotted and drilled holes, as well as different levels of axial preload in the bolts after assembly. The obtained results will be compared with S-N curves of similar categories of components and connections available in current standards. This work also deals with the issue of determining the dynamic load of these bolted connections, as well as problematic aspects in developing the design and conducting experimental testing of these joints. [1]

## 2 Massive Deployment of Renewable Energy

Currently, there is a huge development of renewable energy sources. Among the most important are hydroelectric, wind and solar power plants. The choice of these energy sources usually depends on the geographical and climatic conditions that are characteristic of a given country. As an example, one of the largest photovoltaic power plants in the Czech Republic, which was built near the city of Brno, is presented in Fig. 1.

The solar power plant complex was created under the auspices of an investor, the Brno Solar Park company, and the costs of the entire project reach the amount of 1,7 billion Czech crowns, which means that the financial requirements for 1 MW are around 800 million Czech crowns.

**Parameters of this photovoltaic power plant:**

- area 40 ha,
- number of panels 90,000 pieces

DOI: 10.2478/scjme-2025-0038, Print ISSN 0039-2472, On-line ISSN 2450-5471

- panel output (225 – 280) W
- electric energy,
- total output 21,2 MW.

Fig. 1 Photovoltaic Power Plant in Brno (Czech Republic) - Tuřany airport

Fig. 2 Outdoor Photovoltaic Solar Energy Laboratory (University of Oviedo, Polytechnic School of Engineering of Gijón)

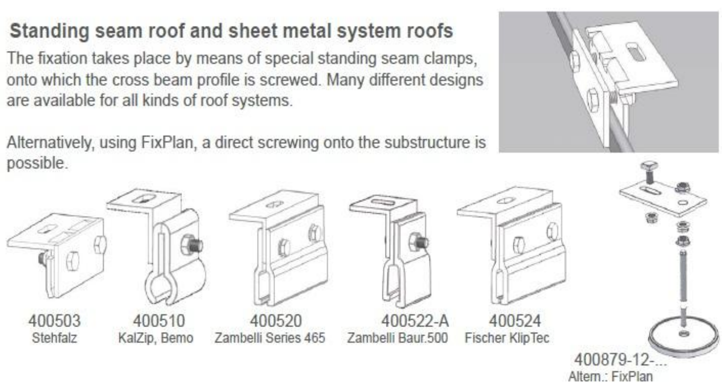


Fig. 3 Methods of Fastening Solar Panels of Photovoltaic Power Plants to a Steel Structure

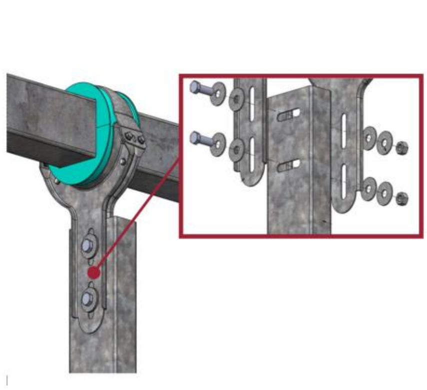

Fig. 4 Fastening the Rotating Beam with Photovoltaic Panels to the Support Column [1]

Used Fasteners:

- HEX HEAD SCREW ISO 4017-M16x50-10.9, (zinc plated? / hot-dip galvanized?),
- HEX NUT ISO 4032-M16-10, (zinc plated? / hot-dip galvanized? / oxidized black coating),
- FLAT WASHERS ISO 7093-16-140HV (zinc plated? /hot-dip galvanized?) - larger contact area, low hardness or

- HEAVY WASHER EN 14399-6-16-300 (370) HV - small contact area, high hardness

The outdoor photovoltaic solar energy laboratory of University of Oviedo, Polytechnic School of Engineering in Gijón, is presented in Fig. 2. The different ways of attaching the photovoltaic panels to the steel support structure and other details of support structure are shown in Fig. 3 and Fig. 4.

Product Parameters

**Photovoltaic Panels**

| Model | Cells Type | Wattage Range | Cells | Size(mm) | Package |
|---|---|---|---|---|---|
| JAM54D30 GB | Mono PERC 182×182mm | 400-425W | 108 (6×18) | 1722×1134×30 | 36pcs/Pallet 936pcs/40HQ |
| JAM72D30 GB | Mono PERC 182×182mm | 540-565W | 144 (6×24) | 2278×1134×30 | 36pcs/Pallet 720pcs/40HQ |
| JAM78D30 GB | Mono PERC 182×182mm | 585-610W | 156(6×26) | 2465×1134×35 | 31pcs/Pallet 496pcs/40HQ |
| JAM54S31 MR | Mono PERC 182×182mm | 380-405W | 108(6×18) | 1722×1134×35 | 36pcs/Pallet 936pcs/40HQ |
| JAM54D40 LB | Mono N-Type 182×182mm | 430-455W | 108 (6×18) | 1762×1134×30 | 36pcs/Pallet 936pcs/40HQ |
| JAM66D45 LB | Mono N-Type 210×210mm | 590-615W | 132 (6×22) | 2382×1134×30 | 36pcs/Pallet 720pcs/40HO |
| JAM72D40 LB | Mono N-Type 182×182mm | 575-600W | 144 (6×24) | 2333×1134×30 | 36pcs/Pallet 720pcs/40HQ |
| JAM78D40 MB | Mono N-Type 182×182mm | 605-630W | 156(6×26) | 2465x1134x35 | 31pcs/Pallet 496pcs/40HQ |

Fig. 5 Standardized Parameters of the Most Commonly Used Photovoltaic Panels

Standardized parameters of the most commonly used photovoltaic panels are shown in Fig. 5 and one possible arrangement of a photovoltaic panels assembly is shown in Fig. 6.

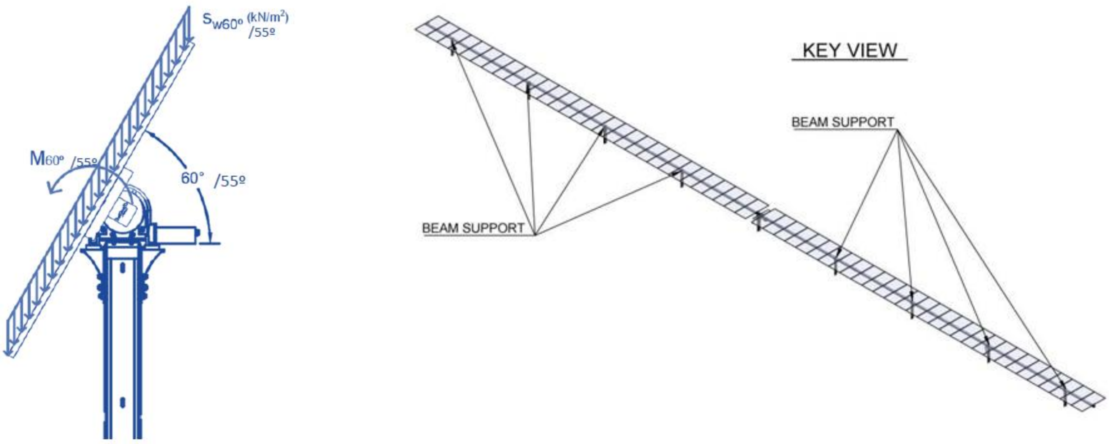


Fig. 6 Assembly of Photovoltaic Panels; Arrangement 2 x 30 Pieces Supported by 9 Columns; Total Weight is 2 x 1 002 kg [1]

## 3 Load on Photovoltaic Panels from Aerodynamic Forces (from Wind)

In calculating wind load on solar panels, was using the American standard ASCE 7-16. A similar calculation procedure is also given in the Spanish standard „Documento Básico SE-AE“. A wind map of the Iberian Peninsula is shown in Fig. 7.

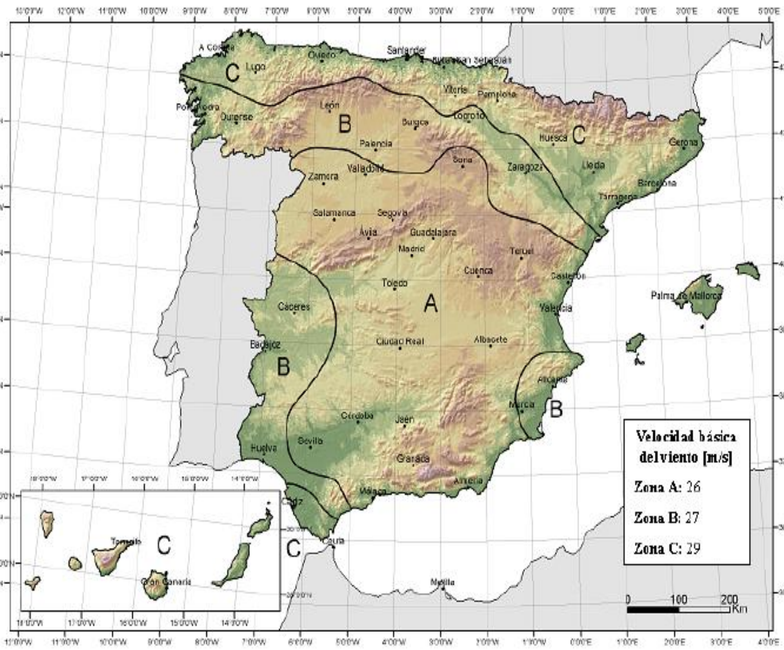


Fig. 7 Wind map of the Iberian Peninsula

In northern Spain, in Asturias, wind speeds reach up to 29 m/s (Fig. 7, zone *C*).

Calculation according to the standard ASCE 7-16 according to the equation (1):

$$p = q_h \cdot G \cdot C_N \tag{1}$$

where: $G$ - gust effect factor, $C_N$ - net force coefficient for open monoslope roof, $C_f$ - net force coefficient for solid signs, $q_h$ - velocity pressure at reference height, h, in psf, given by the formula (2):

$$q_h = 0{,}00256 \cdot K_Z \cdot K_{Zt} \cdot K_d \cdot K_e \cdot V^2 \tag{2}$$

where: $K_z$ - velocity pressure coefficient, $K_{zt}$ - topographic factor, $K_d$ - wind directionality factor, $K_e$ - ground elevation factor, $V$ - basic wind speed in mph.

Calculation according to the Spanish standard “Documento Básico SE-AE” according to the equation (3):

$$q_e = q_b \cdot c_e \cdot c_p \tag{3}$$

where: $q_b$ - the dynamic wind pressure. In simplified form, the value at any location in Spain can be 0,5 kN/m$^2$.

More precise values can be obtained from Annex D depending on the geographical location of the structure, $c_e$ - is the exposure coefficient, which varies with the height of the point under consideration depending on the degree of roughness of the environment where the structure is located, $c_p$ - is a wind or pressure coefficient that depends on the shape and orientation of the surface relative to the wind and, possibly, on the location of the point relative to the edges of that surface.

Note: $G = c_e; C_N = c_p; q_h = q_b; p = q_e$

The basic value of the dynamic wind pressure can be obtained from the expression (4):

$$q_b = 0{,}5 \cdot \delta \cdot v_b^2 = 0{,}5 \cdot 1{,}25 \cdot 29^2 = 525{,}63 N/m^2 \approx 0{,}53 kN/m^2 \quad (4)$$

where δ is the air density and $v_b$ is the basic value of the wind speed.

The density of air depends, among other things, on altitude, ambient temperature and the proportion of suspended water. A value of 1,25 kg/m$^3$ can generally be assumed. In locations very close to the sea, where dew is very likely, the density may be higher.

**Tabla 3.4. Valores del coeficiente de exposición $c_e$**

| | Grado de aspereza del entorno | Altura del punto considerado (m) | | | | | | | |
|---|---|---|---|---|---|---|---|---|---|
| | | 3 | 6 | 9 | 12 | 15 | 18 | 24 | 30 |
| I | Borde del mar o de un lago, con una superficie de agua en la dirección del viento de al menos 5 km de longitud | 2,4 | 2,7 | 3,0 | 3,1 | 3,3 | 3,4 | 3,5 | 3,7 |
| II | Terreno rural llano sin obstáculos ni arbolado de importancia | 2,1 | 2,5 | 2,7 | 2,9 | 3,0 | 3,1 | 3,3 | 3,5 |
| III | Zona rural accidentada o llana con algunos obstáculos aislados, como árboles o construcciones pequeñas | 1,6 | 2,0 | 2,3 | 2,5 | 2,6 | 2,7 | 2,9 | 3,1 |
| IV | Zona urbana en general, industrial o forestal | 1,3 | 1,4 | 1,7 | 1,9 | 2,1 | 2,2 | 2,4 | 2,6 |
| V | Centro de negocio de grandes ciudades, con profusión de edificios en altura | 1,2 | 1,2 | 1,2 | 1,4 | 1,5 | 1,6 | 1,9 | 2,0 |

Fig. 8 Table for Determining the Coefficient $c_e$ (exposure coefficient)

$G = c_e = 2{,}1$

**Net Force Coefficient, $C_f$ – Tilt Angle > 45°**

We will consider the ground-mounted solar panel as a solid sign for tilt angle greater than 45° now.

Let's say that our solar panel tilt angle was changed to **60°**. We need to use the vertical projection of the solar panel and consider it as a solid sign with the velocity pressure calculated up to the top of this projection.

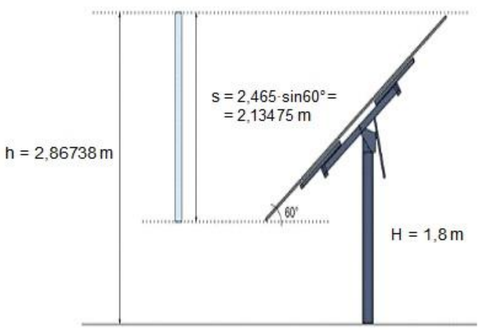


Fig. 9 Location of the Photovoltaic Panel Relative to the Ground

Photovoltaic panel dimensions:

$B$ = 1,134 m; $L$ = 2,465 m; $s/h$ = 2,13475 / 2,86738 = 0,7445; $B/s$ = 1,134 / 2,13475 = 0,5312

| Force Coefficients, $C_1$, for Case A and Case B | | | | | | | | | | | | |
|---|---|---|---|---|---|---|---|---|---|---|---|---|
| Clearance Ratio $s/h$ | Aspect Ratio, $B/s$ | | | | | | | | | | | |
| | ≤ 0.05 | 0.1 | 0.2 | 0.5 | 1 | 2 | 4 | 5 | 10 | 20 | 30 | ≥45 |
| 1 | 1.50 | 1.70 | 1.65 | 1.55 | 1.45 | 1.40 | 1.35 | 1.35 | 1.30 | 1.30 | 1.30 | 1.30 |
| 0.9 | 1.85 | 1.75 | 1.70 | 1.60 | 1.55 | 1.50 | 1.45 | 1.45 | 1.40 | 1.40 | 1.40 | 1.40 |
| 0.7 | 1.90 | 1.85 | 1.75 | 1.70 | 1.65 | 1.60 | 1.60 | 1.55 | 1.55 | 1.55 | 1.55 | 1.55 |
| 0.5 | 1.95 | 1.85 | 1.80 | 1.75 | 1.75 | 1.70 | 1.70 | 1.70 | 1.70 | 1.70 | 1.75 | 1.75 |
| 0.3 | 1.95 | 1.90 | 1.85 | 1.80 | 1.80 | 1.80 | 1.80 | 1.80 | 1.80 | 1.85 | 1.85 | 1.85 |
| 0.2 | 1.95 | 1.90 | 1.85 | 1.80 | 1.80 | 1.80 | 1.80 | 1.80 | 1.85 | 1.90 | 1.90 | 1.95 |
| ≤ 0.16 | 1.95 | 1.90 | 1.85 | 1.85 | 1.80 | 1.80 | 1.85 | 1.85 | 1.85 | 1.90 | 1.90 | 1.95 |

Fig. 10 Table for Determining the Coefficient $C_f$ (Net Force Coefficient)

From the tabulated values of $C_f$ in Fig. 10, we will interpolate the known values of B/s equal to 0,5 and 1, and s/h equal to 0,9 and 0,7.

$C_f$ = 1,672

In calculating wind load on solar panels with tilt angle > 45°, we will be using equation (1) with coefficient $C_f$, hence, the wind loads on ground-mounted solar panels we calculate from the equation (5):

$$p = q_h \cdot G \cdot C_f = 0{,}53 \cdot 2{,}1 \cdot 1{,}672 = 1{,}86094\ kN/m^2 \quad (5)$$

Therefore, the wind loads on ground-mounted solar panels when applied.

The design wind pressure for the solar panel as solid sign – applied to the vertical projection.

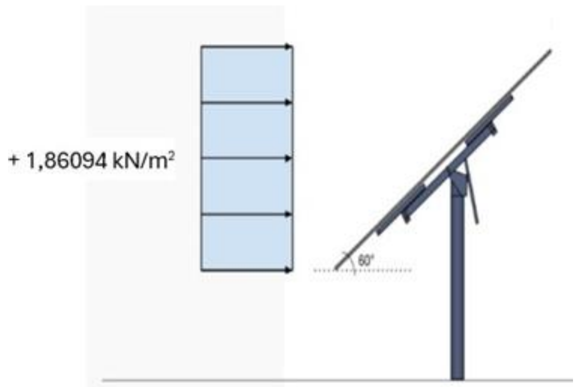


Fig. 11 Load on the Photovoltaic Panel from Dynamic Wind Pressure

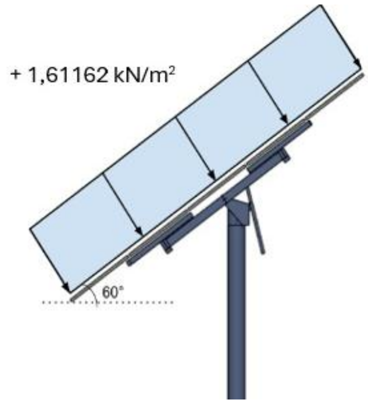


Fig. 12 Load on the Photovoltaic Panel from Dynamic Wind Pressure when Applied Vertical Projection

The converted design wind pressure for the solar panel as solid sign – applied to the surface of the solar panel.

Area of one photovoltaic panel: $A = L \cdot H = 2{,}465 \cdot 1{,}134 = 2{,}79531 \approx 2{,}8$ m²

Total force $F_{C1}$ [kN] acting on one panel for panel load case $A$:

$F_{C1} = p_A \cdot A = 1{,}61162 \cdot 2{,}8 \approx 4{,}51254$ kN

Total force $F_{C60}$ [kN] acting on 60 panels for panel load case A:

$F_{C60} = 60 \cdot p_A \cdot A = 60 \cdot 1{,}61162 \cdot 2{,}8 \approx 270{,}7522$ kN

Force $R_{COL}$ [kN] acting on the upper end of a single column for panel load case $A$: (9 columns)

$R_{COL} = F_{C60} / 9 = 270{,}7522 / 9 \approx 30{,}0836$ kN

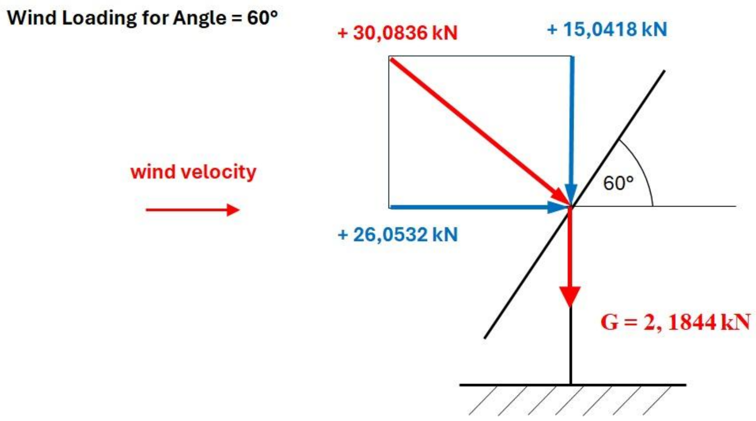


Fig. 13 Forces Acting on the Upper End of a Single Column for Panel Load Case $A$

## 4 Assessment of Designed Slotted Prestressed Bolted Joints

First, the basic equation (6) of the load-bearing capacity of the clamping joint is presented:

$$T \geq k \cdot (4 \cdot F_r) = 4 \cdot F_T = 4 \cdot \mu \cdot F_o \quad (6)$$

where: $T$ – total friction force; $F_T$ – friction force on one contact surface; $F_r$ – maximum radial force on one bolt joint; $F_o$ – operating preload of the bolt; $k$ – coefficient of safety of the friction joint; μ – coefficient of friction between plates.

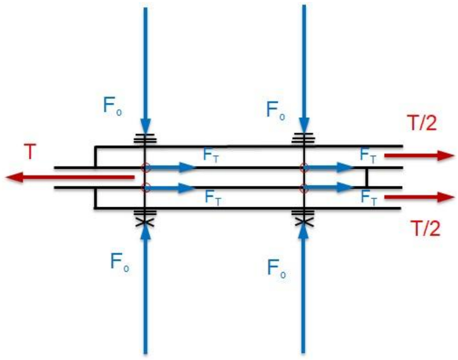


Fig. 14 Analytical Computational Model of the Clamping Joint

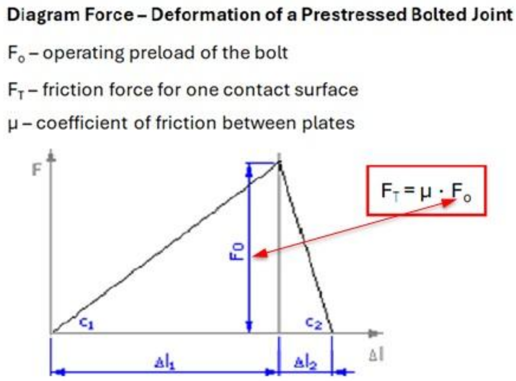


Fig. 15 Diagram Force – Deformation of a Prestressed Bolted Joint

**Used materials:**

BOLTS + NUTS

Bolt - strength class 10.9, galvanized (HEX HEAD SCREW ISO 4017-M16x50-10.9),

Nut – strength 10, galvanized (HEX NUT ISO 4032-M16-10).

PLATES

Steel S350GD+ZM310, S350GD - High Anti-corrosion, Zn-Al-Mg Alloy Coating,

ZM310 - Zinc Aluminum Magnesium Steel for Building Materials

The use of high-strength fasteners in combination with sheets of relatively low hardness and with washers of low surface hardness appears to be structurally unsuitable.

FLAT WASHERS ISO 7093-16-140 HV (washer 1)

(zinc plated/hot dip galvanized) - larger contact area, low hardness, (see Fig. 16).

The use of hard washer also led to considerable plastic deformations of the surface of sheets with low surface hardness.

HEAVY WASHER EN 14399-6-16-300(370) HV (washer 2)

- small contact area, high hardness (see Fig. 16).

Fig. 16 Due to the large bending deformation of the **washer 1** (on the left side), the actual contact surface is smaller and therefore the contact pressure will be much higher; due to the very small contact area of the **washer 2**, (on the right side) the contact pressure is also too high

| Strength calculations of bolted joints M16x50 (10.9) | | | |
|---|---|---|---|
| **Strength calculation parameters** | **$F_r$=9 375 N; f=0,2; $k_s$=1,2; $k_r$=1** | **$F_r$=9 375 N; f=0,15; $k_s$=1,2; $k_r$=1** | **Units** |
| **Strength check of the connection in working state** | | | |
| Operating prestressing of the bolt | 46 875,18 | 62 500,18 | [N] |
| Resulting reduces stress in the bolt core (HMH) | 338,35 | 443,96 | [N·mm$^{-2}$] |
| Static safety coefficient of the bolt | 2,78 | 2,12 | [1] |
| Tightening torque | 199,49 | 245,97 | [N·m] |
| Contact pressure under the bolt head (nut) | 236,84 | 315,78 | [MPa] |
| **Strength check of the connection in the assembly state** | | | |
| Assembly preload of the bolt | 67 060,00 | 82685,00 | [N] |
| Resulting reduces stress in the bolt core (HMH) | 532,04 | 656,00 | [N·mm$^{-2}$] |
| Contact pressure under the bolt head (nut) | 338,82 | 417,77 | [MPa] |
| **Strength check of connections for maximal prestressing** | | | |
| Maximum operating presstresing of the bolt | 67 060,00 | 82685,00 | [N] |
| Resulting reduces stress in the bolt core | 456,27 | 562,58 | [N·mm$^{-2}$] |
| Maximum contact pressure under the bolt head (nut) | 338,82 | 417,77 | [MPa] |
| **Assembly parameters of the connection** | | | |
| Maximum operating presstresing of the bolt for $\alpha_A$=1,6 | 107 296,00 | 132 296,00 | [N] |
| Minimum operating presstresing of the bolt | 67 060,00 | 82 685,00 | [N] |
| Resulting reduces stress in the bolt core (assembly) | 882,01 | 1 087,51 | [N·mm$^{-2}$] |
| Resulting reduces stress in the bolt core (working st.) | 621,61 | 793,41 | [N·mm$^{-2}$] |
| Static safety coefficient of the bolt | 1,51 | 1,18 | [1] |
| Maximum contact pressure under the bolt head (nut) | 440,13 | 566,45 | [MPa] |
| Minimum possible tightening torque | 175,40 | 216,27 | [N·m] |
| Maximum possible tightening torque | 357,76 | 441,11 | [N·m] |

Fig. 17 Strength Calculations of Bolted Joints M16x50 (strength class 10.9), SW “MITCalc”

With more precise assembly we can consider a lower value of the tightening factor $\alpha_A$.

## 5 FEM Analyzes of Used Prestressed Slotted Bolted Joints

FEM analyzes of the tension of the designed slotted prestressed bolted joints for different values of the axial preload of the bolts were also carried out. The original version of the clamp connection was designed with two bolts and two contact surfaces. The modified version then only has one bolt and two contact surfaces [1-3].

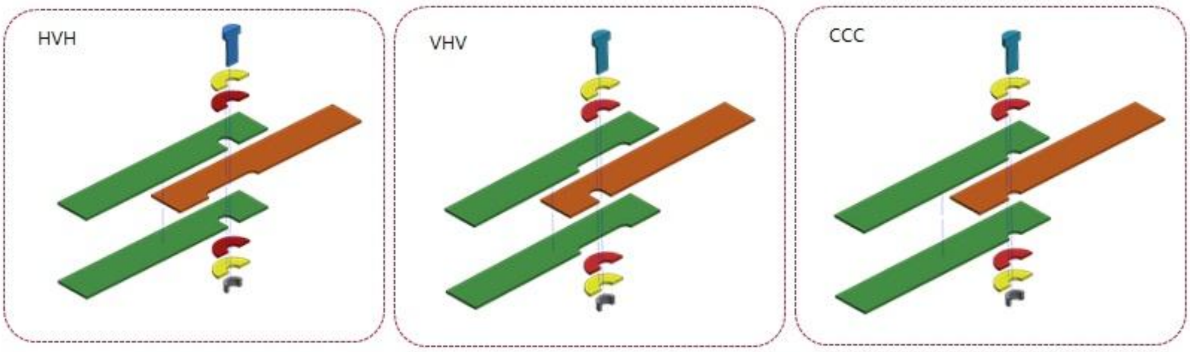


Fig. 18 3D Models of Different Connection Layouts and Test Samples after Modification (with one bolt and two contact surfaces) [1]

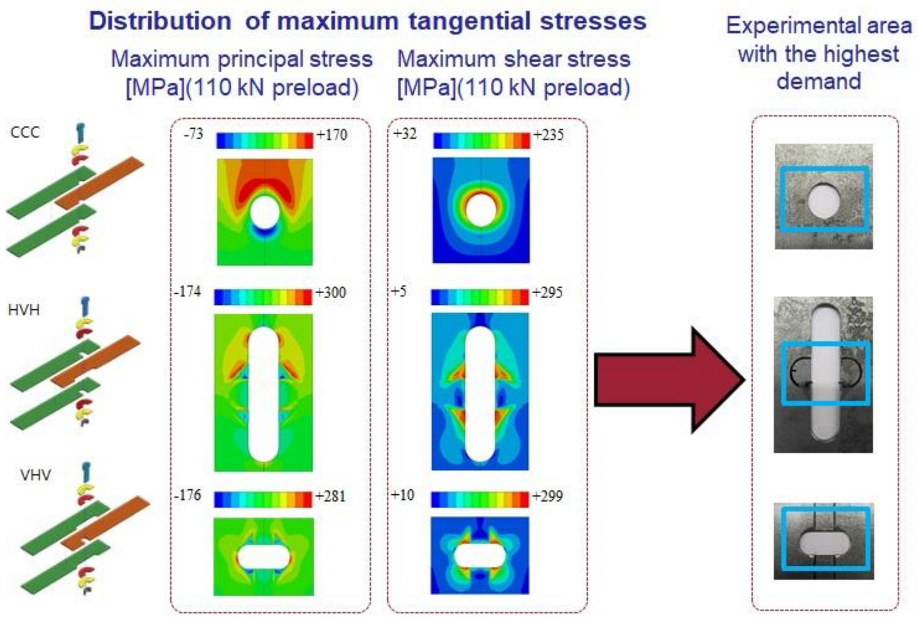


Fig. 19 FEM Stress Analyzes Results for Clamped Joint after Modification (with one bolt and two contact surfaces) [1]

## 6 Experimental Verification of the Bearing Capacity of Prestressed Slotted Bolted Joints and Fatigue Damage Resistance

Load-bearing capacity tests (sliding tests) of individual clamped joint variants were carried out, as well as fatigue tests. No fatigue fracture occurred in any of the fatigue tests carried out.

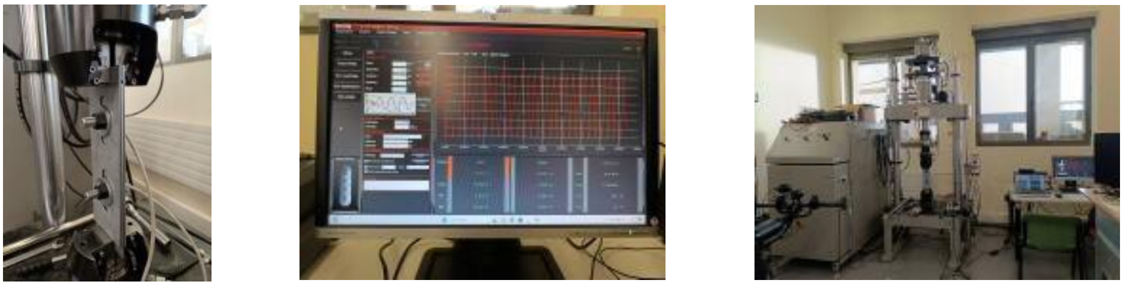

Fig. 20 Experimental Verification of the Fatigue Resistance (Walter&Bai servo-hydraulic testing machine)

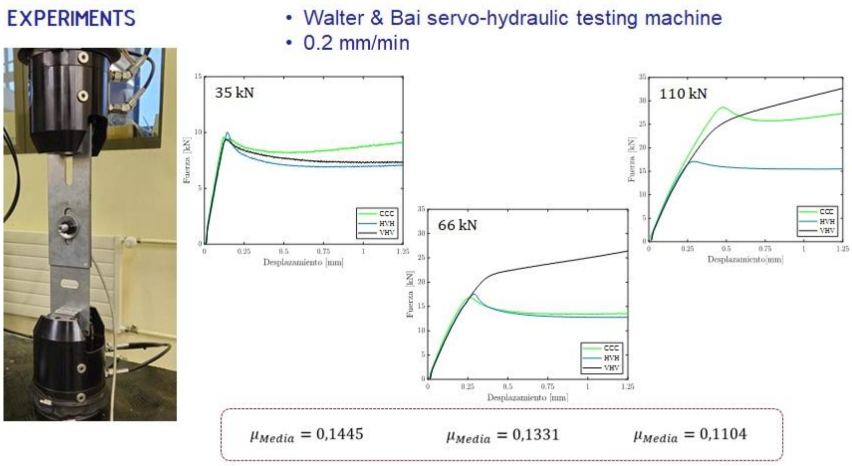


Fig. 21 Sliding Tests Results and Average Value of the Coefficient of Friction [1]

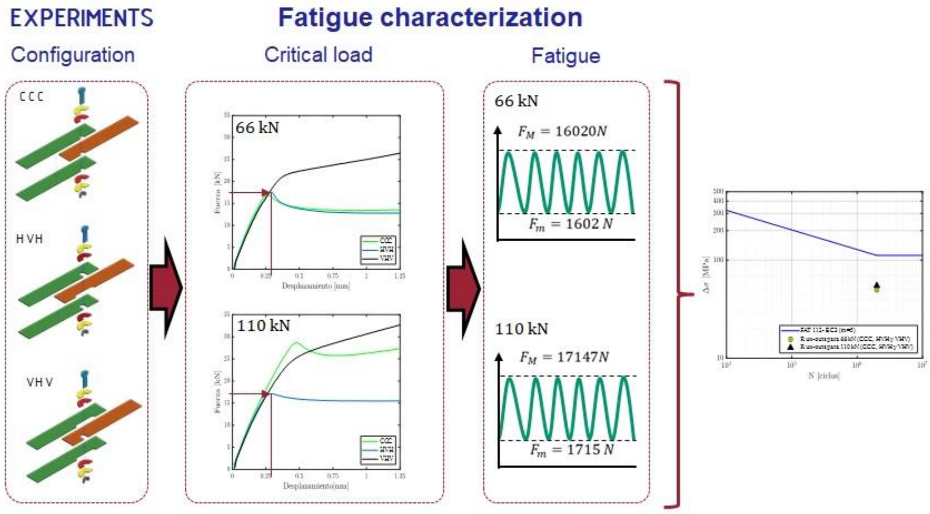


Fig. 22 Fatigue Characterization of Prestressed Slotted Bolted Joints [1]

## CONCLUSION

In none of the realized experiments conducted did fatigue fracture occur in connection with fretting corrosion [4,5].

The solved project was concluded with the conclusion that the proposed structural solution of the prestressed bolted joint was satisfactory.

In Fig. 21, it is easy to see how, with increasing axial preload in the bolt, the bearing capacity of the clamp connection also increases.


### Acknowledgements

Thanks go to my son, Ing. Antonín Kanaval, and all other colleagues in Spain from the University of Oviedo, Polytechnic Faculty of Engineering in Gijón for their support and the materials provided for the project. Financial support from the Rectorate of the Czech Technical University in Prague within the framework of Erasmus mobility. Participant agreement no. STT029/24/25.


## REFERENCES


[1] Díaz-Salamanca, D., Kanaval, A., Muñiz-Calvente, M., Pelayo, F., Kanaval, J. "Fatigue Performance of Hot-dip Galvanized Bolted Joints: Influence of Geometry and Preload Conditions", 41st Congress of the Spanish Fracture Group, March 26-28, Vitoria, Department of Construction and Manufacturing Engineering, Gijón 33203, University of Oviedo, Spain, **2025**.

[2] Welch, M. "Mechanisms of Bolt Preload Relaxation Arising from In-Plane Loads and Bolt Bending", Strojnícky časopis – Journal of Mechanical Engineering 74(3), pp. 145 – 172, **2024**. DOI: 10.2478/scjme-2024-0041

[3] Welch, M. "A Paradigm for the Analysis of Preloaded Bolted Joints", Strojnícky časopis – Journal of Mechanical Engineering 69 (1), pp. 143 – 152, **2019**. DOI: 10.2478/scjme-2019-0012.

[4] De Azevedo, F., Erick, S., Guidi, S. "Influence Analysis of Washers Material in Fatigue Life of Bolted joints", **2018**.

[5] European Commission, Eurocode 3: Design of steel structures - Part 1-9: Fatigue. https://eurocodes.jrc.ec.europa.eu/EN-Eurocodes/eurocode-3-design-steel-structures, **2005**.